Journal of Applied Electrochemistry
https://doi.org/10.1007/s10800-023-01975-z

RESEARCH ARTICLE

Synthesis of Nb_2O_5/C for H_2O_2 electrogeneration and its application for the degradation of levofloxacin

Ricardo Bertholo Valim[1,2] · Jussara Fernandes Carneiro[1] · Julio César Lourenço[1] · Peter Hammer[3] · Mauro Coelho dos Santos[4] · Liana Alvares Rodrigues[2] · Rodnei Bertazzoli[5] · Marcos Roberto de Vasconcelos Lanza[1] · Robson da Silva Rocha[2]

Received: 21 June 2023 / Accepted: 14 August 2023

Abstract

The present work sought to investigate H_2O_2 generation using a gas diffusion electrode (GDE) composed of carbon with niobium oxide for levofloxacin (LEVO) degradation. Results showed that the oxide formed was Nb_2O_5 (crystallographic structure was confirmed by XRD; chemical composition detected by XPS), and the increase in the Nb/C ratio led to more crystalline structure and higher crystallite size. The carbon with 5% Nb_2O_5 presented an average particle size of 5.6 nm, and this material led to the generation of the highest amount of H_2O_2 (317.6 mg L^{-1}). The C/5% Nb_2O_5-modified GDE was applied for the degradation of LEVO in an acid medium in the presence and absence of Fe^{2+} ions. Long-term experiments conducted to analyze the time required for the total removal of LEVO showed that 96% of LEVO and 66% of organic load were removed in 270 min of treatment at the current density of 100 mA cm^{-2}.

Graphical abstract

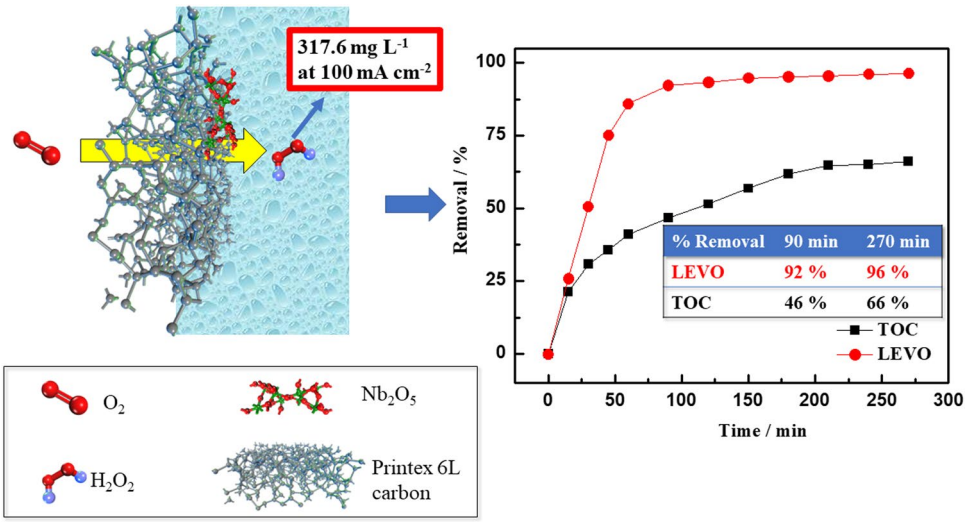

Keywords Levofloxacin · Antibiotic degradation · Hydrogen peroxide · Gas diffusion electrode · Advanced oxidation process

Extended author information available on the last page of the article

Published online: 29 August 2023

1 Introduction

The rapid development of society in the last century has resulted in great advances in human activity, with huge progress in industrial, technological, medicine, and food production; these massive advances have, at the same time, caused significant impacts on the environment [1] showed that while the relationship between the economy, society, and the environment is not always evident, one factor is clear in this relationship: environmental degradation [1].

One of the visible aspects of societal development is population growth, which goes hand in hand with the increase of large urban centers [1]. Highly populated regions tend to suffer considerably from the depletion of natural resources, and water resources in these regions are significantly impacted, where the areas with high population density largely experience a decrease in both water supply and water quality [2].

The scenario for the coming years shows that a greater portion of the population will be living in large urban centers [1], and this may directly impact the availability and quality of water in these regions [2]; in this sense, it is essentially crucial to control the vectors of environmental contamination, knows their origins, and understand the interaction of these contaminants [3–6].

It is undoubtedly clear that considerable attention needs to be paid when it comes to the disposal of medicine into the environment; this is because the exposure of humans and other living beings to natural waters contaminated by this class of compounds has been found to pose serious health risks, regardless of the low concentrations of the compounds (ng L^{-1} or µg L^{-1}) [3–6].

In this context, public water and sewage treatment systems must account for the presence of emerging pollutants in raw water or sewage during the treatment processes, and it must be borne in mind that conventional techniques may not be efficient when it comes to removing specific emerging contaminants. Different works analyzed the presence of drugs in some Brazilian water supply systems; the authors detected the presence of 12 drugs in surface water used for public consumption, and out of these 12 drugs, 6 drugs were identified after the water treatment process [7, 8].

Becker et al. identified 43 drugs in the sewage of a hospital in the State of Rio Grande do Sul in Brazil as part of work to identify metabolites [6]. Pivetta et al. studied the degradation/removal of drugs in water samples from a sewage treatment plant in the city of Campinas in Brazil; the authors analyzed 10 medications with psychotropic activity, out of which 8 were identified before and after the water treatment in the sewage treatment plant [8]. Based on the findings of Pivetta et al., the only drug that was totally removed after the water treatment process was sertraline. The authors recorded minimal removal rates or zero removal rates for the drugs investigated; in other words, the sewage treatment plant was incapable of removing the drugs from the water samples [8].

Epold, Trapido, and Dulova [9] and Hamdi El Najjar et al. [10] cited that many antibiotics have high resistance to biological treatment processes commonly used in cities, such as LEVO, indicating that these substances can cause long-term concerns due to toxicity in water bodies and cause bacterial resistance. Mustafa and Oladipo [11] cited the high solubility of some drugs and the consequent increase in their metabolites in the environment, which can cause serious problems associated with resistance to these drugs and environmental toxicity [12, 13].

Considering the limitations of conventional water and sewage treatment processes, where drugs, among many other contaminants, are detected in sewage/wastewater before and after treatment, as well as in surface water and drinking water for human consumption [3–6], one does not need to overemphasize the importance of developing efficient treatment techniques which are capable of the following: (i) maximizing the removal of these compounds in wastewater before they reach the sewerage system; (ii) removing/degrading the compounds during the sewage treatment stage; or (iii) effectively removing the compounds in the water treatment process.

Several works published in the literature have proposed different techniques for the removal or degradation of drugs, among these techniques include advanced oxidative processes [3–6]. According to Wu and Hu [14], advanced oxidative processes have enormous advantages over other techniques when it comes to the degradation of pharmaceutical compounds because they can mineralize drugs completely using small working areas [14–18]. Hassani et al. listed several processes for the degradation of organic pollutants, such as photo-Fenton, sono-Fenton, and electro-Fenton, and the latter process is indicated as very promising, mainly due to the in situ generation of hydroxyl radicals [19].

Ighalo et al. showed that under advanced oxidative processes, applying hydrogen peroxide (H_2O_2) with a small amount of Fe^{2+} ions leads to the efficient removal of drugs in water matrice [16].

In large-scale processes, commercial H_2O_2 can be a serious problem since storing large amounts of H_2O_2 requires controlled environmental conditions and careful handling procedures. In view of that, electrochemical techniques using gas diffusion electrode (GDE) are highly efficient H_2O_2 synthesis in situ [20] where the use of electrochemical technologies allows controlling the H_2O_2 generation in view of the real need in the process under study; this characteristic is highlighted by Hassani et al. [18].

H_2O_2 electrochemical synthesis is complex [21]; the use of GDE allows one to perform the synthesis of H_2O_2 at room temperature/pressure and in direct contact with the pollutants [20]. A number of works published in the literature have demonstrated the efficiency of GDE when it comes to O_2 reduction in H_2O_2 synthesis [22–26]. GDE is a versatile electrode applied in H_2O_2 generation; this electrode can be constructed using a catalytic mass composed of carbon only [20] or carbon modified with different substances [25, 27]. Silva et al. reported the production of 240 mg L^{-1} of H_2O_2 after 90 min, using f iron (II) phthalocyanine as a modifier of carbon black [28]. Antonin et al. reported that GDE modified with W@Au Nanostructures using Vulcan XC-72R produced 120 ppm of H_2O_2 after 120 min using a potential of − 1.3 V [29]. Carneiro et al. modified Printex 6 L with nanostructured Ta_2O_5 and obtained a production of 29.7 mg L^{-1} of H_2O_2 after 120 min [22]. Valim et al. reported the production of 281.6 mg L^{-1} of H_2O_2 after 120 min using a GDE modified with Ru-Nb oxides [30]. The use of niobium to modify the carbon to obtain Nb_2O_5/C is of interest, as the use of this oxide is reported in the literature as having an effect of shifting the onset in the potential to fewer negatives potentials and also increasing the selectivity toward the 2-electrons pathway, increasing the generation of the H_2O_2 [30, 31].

In regards to LEVO degradation, some studies can be observed in the literature: Zhang et al. [32] used a $BiVO_4$/CO_3^{2-}–$Bi_2O_2CO_3$ heterojunction for degradation of LEVO under visible light, and they achieved a degradation of 78% after 90 min. Xu et al. [33] used a boron-doped diamond electrode in pulse electrochemical oxidation for the degradation of LEVO and reached 94.4% degradation after 120 min. Busaidi et al. [34] used photocatalytic $Cd_xZn_{(1-x)}O$ for LEVO degradation under solar light irradiation and reached 96% degradation after 240 min. Jandaghian et al. [35] compared Ag-deposited over ZnO and TiO_2 materials for LEVO degradation under UV/visible radiation, reaching over 90% LEVO degradation under UV radiation.

Considering the importance of the removal of organic pollutants in water and environmental matrices and the need for the development of efficient techniques that are highly capable of decontaminating drug-contaminated water, the present work seeks to investigate the electrogeneration of hydrogen peroxide in GDEs made up of carbon modified with niobium oxide and the application of the proposed technique for the degradation of LEVO. The novelty of the presented work is obtaining a Nb_2O_5/C GDE that successfully degrades LEVO, producing H_2O_2 in situ for the electro-Fenton degradation process and using a commercial LEVO as the degradation compound.

2 Experimental

2.1 Preparation of Nb_2O_5/C nanoparticles

Nb_2O_5 nanoparticles supported on Printex L6 carbon (Evonik Co.) were synthesized by thermal decomposition of a polymeric precursor using niobium ammonium oxalate ($NH_4[NbO(C_2O_4).H_2O$ (purchased from Companhia Brasileira de Metalurgia e Mineração—CBMM, Brazil) was used as salt precursor. The salt was placed in a mixture containing ethylene glycol and citric acid in a molar ratio of 1:10:40, respectively, at 60 °C. After homogenization, Printex L6 carbon was added to the mixture, and the suspension formed was subjected to magnetic stirring for 20 min. After that, the resulting dispersion was calcined in air at 500 °C for 30 min. The mass proportion of niobium and carbon (Nb/C) applied was 0.5, 1.0, 3.0, 5.0, 8.0, 10, and 15% (w/w).

2.2 Physical characterization

X-ray fluorescence (XRF) measurements were performed using MiniPal 4 apparatus model PW 4024 with a PANalytical B.V. rhodium X-ray tube (Almelo, the Netherlands). Powder X-ray diffraction (XRD) patterns were obtained from a Rigaku diffractometer operated under a Cu-K_α radiation source ($\alpha = 1.54056$ Angstrom) at a voltage power of 40 kV and current density of 80 mA. The compounds formed were identified based on a comparison with standard compounds using the International Center of Diffraction Data (JCPDS) database.

TEM analyses were carried out using a JEOL transmission electron microscope, model JEM-2100, operated at 200 kV.

X-ray photoelectron spectroscopy (XPS) analysis was carried out using a commercial spectrometer at a pressure of less than 10^{-7} Pa (UNI-SPECS UHV System, Berlin, Germany). The analysis was performed using the Mg-K_α line ($h\nu = 1253.6$ eV) and analyzer pass energy of 10 eV. The inelastic background of the Nb 3d, C 1s, and O 1s electron core-level spectra was subtracted using Shirley's method. The composition (at.%) of the near-surface region was determined at an accuracy of ± 10% from the ratio of the relative peak areas corrected by Scofield's sensitivity factors for the corresponding elements. The binding energy scale of the spectra was corrected using the C 1s hydrocarbon component at a fixed potential of 285.0 eV. The spectra were fitted without constraints using multiple Voigt profiles. The full width at half maximum (FWHM) varied between 1.2 and 2.1 eV, and the accuracy of the peak positions was ± 0.1 eV.

2.3 Electrochemical characterization

The electrochemical experiments were conducted using an Autolab PGSTAT 128 N potentiostat/galvanostat (Metrohm) with a rotating ring-disk electrode (RRDE) (Pine Instruments). The RRDE consisted of a central glassy carbon disk and a platinum ring with a collection efficiency of $N = 0.37$. The working electrodes were prepared as described in [26]; the electrodes were prepared by dispersing 1 mg of each material studied and carbon with 20% Pt (ETEK) in 1 mL of water. After homogenization, 25 µL aliquots of the solution were placed on the glassy carbon disk and dried under N_2 flow. The experiments were performed using a supporting electrolyte which consisted of 0.1 mol L^{-1} K_2SO_4, where the pH was adjusted to 2 using H_2SO_4. A platinum foil was employed as the auxiliary electrode, and Ag/AgCl electrode was used as the reference electrode.

The microlayers were electrochemically characterized by cyclic voltammetry (CV) using the supporting electrolyte saturated with nitrogen gas in the potential range of + 0.6 to − 0.6 V and at a scan rate of 10 mV s^{-1}. Subsequently, linear voltammetry (LV) measurements were performed using the supporting electrolyte solution saturated with oxygen gas. The voltammograms were obtained in the potential range of + 0.4 to − 0.8 V and at a scan rate of 5.0 mV s^{-1}. A potential of + 1.0 V was applied to the Pt ring electrode, and this was used for the detection of H_2O_2 formed on the microlayer.

2.4 Electrochemical generation of H_2O_2 on GDE

The quantification of the H_2O_2 produced during the oxygen reduction reaction (ORR), using either unmodified carbon or 5% Nb_2O_5/C (w/w) as a conductive matrix. The GDEs (20 cm^2) were prepared based on the procedure described in previous studies [3–6]; under the procedure employed, polytetrafluoroethylene (PTFE) was used as a hydrophobic binder (20% (w/w) of a 60% aqueous dispersion—Dyneon TF 5035, 3 M) and metallic screens were used for current collection. The GDEs were constructed by the hot-pressing mechanism as described in the literature [20].

The electrogeneration of H_2O_2 was performed in a conventional electrochemical cell using 0.1 mol L^{-1} K_2SO_4, at pH 2 (adjusted by H_2SO_4), as a supporting electrolyte. A platinum plate was used as an auxiliary electrode, and Ag/AgCl electrode (10 cm^2) was used as the reference electrode. During the electrolysis, 0.5 mL of the electrolyte solution was added to 4 mL of 2.4×10^{-3} mol L^{-1} $(NH_4)_6Mo_7O_{24}$ in 0.5 mol L^{-1} H_2SO_4, and the absorbance of the resulting solution was measured at 350 nm. The electrolysis was carried out using Autolab PGSTAT 30 potentiostat/galvanostat (Metrohm) with a high current module at constant current density in the 10 to 150 mA cm-2 range for 90 min.

2.5 LEVO degradation using Nb_2O_5/C-GDE

The degradation experiments were carried out using the same conditions applied for the H_2O_2 generation experiments (current density range: 10 to 150 mA cm^{-2}; time: 90 min), with the application of 0.1 mol L^{-1} K_2SO_4 at pH 2 (adjusted by using concentrated H_2SO_4) as supporting electrolyte in the presence and absence of 0.1 mmol L^{-1} $FeSO_4$ with 10 mg L^{-1} of LEVO using a commercial compound.

The samples collected from the degradation experiments were analyzed by high-performance liquid chromatography (HPLC) using a Shimadzu Prominence LC 20 AT instrument fitted with a C-18 column (250 × 4.6 mm id; 5 µm) at 270 nm. The mobile phase employed consisted of 0.5% formic acid applied in water (solvent A) and acetonitrile (solvent B) applied at a flow rate of 1 mL min^{-1}. The elution program employed was as follows: 0–0.5 min, 15% B (isocratic); 0.50–0.51 min, 15–30% B (step); 0.51–7.50 min, 30–75% B (linear gradient); and 7.5–12.00 min, 75–15% (linear gradient). A Shimadzu TOC-VCPH analyzer was used to monitor the removal of organic carbon.

3 Results and discussion

3.1 Structural, morphological characterization

Figure S1 shows the X-ray fluorescence emission spectra of the niobium incorporated into the Printex L6 carbon in lines K_α 16,529 keV and K_β 18,621 keV. Each metal has energy values that are typically characteristic of the fluorescence emission; for niobium, the values are in K_α 16,58 keV and K_β 18,62 keV [36]. As can be observed, the experimental values agree with the tabulated values; this shows that the metal has been efficiently incorporated into the carbon support.

The XRD patterns obtained for the Printex L6 and 15% Nb/C electrocatalysts are shown in Fig. 1.

The XRD patterns show the typical crystalline characteristics of the Nb_2O_5 orthorhombic phase for Printex L6 carbon modified with niobium based on the JCPDS data 30–873. The intensity of the peaks related to the Nb_2O_5 phase increased when the concentration of the metal was increased. It's also noted that peaks became well defined, with lower full width at half maximum (FWHM), indicating greater crystallization when the Nb_2O_5 concentration is increased in the material. The crystallite size was calculated using Rietveld analysis in the HighScore Plus software. The instrumental broadening was discounted using a Si standard measured at the same instrument for the analysis. For the 15% Nb_2O_5/C electrocatalyst presented in Fig. 1, it was observed that the crystallite size of 15.2 nm is the largest crystallite among the studied compositions.

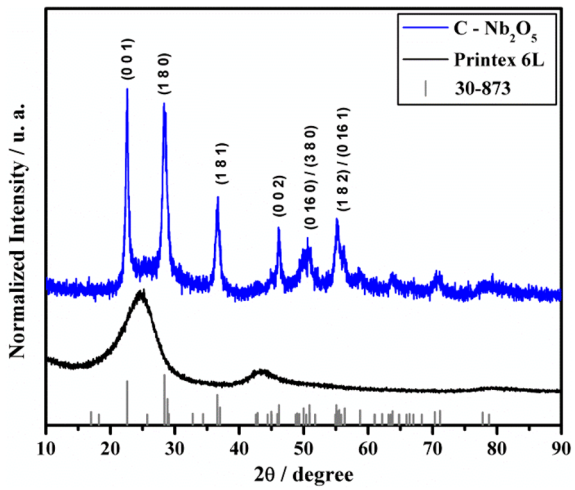

Fig. 1 JCPDS characteristics of the Nb_2O_5 phase and XRD patterns of Printex L6 and 15% Nb/C electrocatalyst

Using the polymeric precursor method under similar experimental conditions for the synthesis of niobium oxide, Carneiro et al. [31] obtained Nb_2O_5 through the application of graphene. Trevelin et al. [36] produced similar Nb_2O_5 particles supported on carbon Printex 6 L under similar synthesis conditions. Thus, the synthesis process presented in this work is efficient for obtaining Nb_2O_5 and is perfectly in line with the synthesis processes reported in the literature.

Figure 2 shows the TEM image of Nb_2O_5 supported on carbon. As can be observed, Nb_2O_5 nanoparticles are well distributed on the carbon support. Figure 2C shows the histogram with mean particle size distribution of 5.6 + 0.7 nm (presented in Fig. 2B). This value reasonably agrees with XRD presented data since XRD peaks with higher FWHM, i.e., less crystalline material, should present smaller crystallite size.

The electron diffraction pattern shows the diffraction halos related to the main planes of Nb_2O_5; the interplanar distances of 3.93 Å, 3.14 Å, and 2.45 Å correspond to the (001), (180), and (181) planes, respectively. The interplanar distance presented in Fig. 2D agrees with the XRD pattern; furthermore, the diffuse ring observed in the electron diffraction pattern image is typically characteristic of the amorphous carbon support. The image in Fig. 2E related to the Nb_2O_5 overlayer is not entirely uniform; this is likely due to Bragg contrast effects caused by the differing orientations of the Nb_2O_5 crystallite planes, which are associated with the incident electron beam.

The 5.0% Nb/C electrocatalyst presented a small average particle size, which is in agreement with the XRD data. This electrocatalyst exhibited a less intense broad peak pattern and a smaller average crystallite size compared to the 15% Nb/C electrocatalyst. The decrease in particle size contributed to an increase in the adsorption of oxygenated species on the catalyst surface [22, 31, 36], and this plays a major

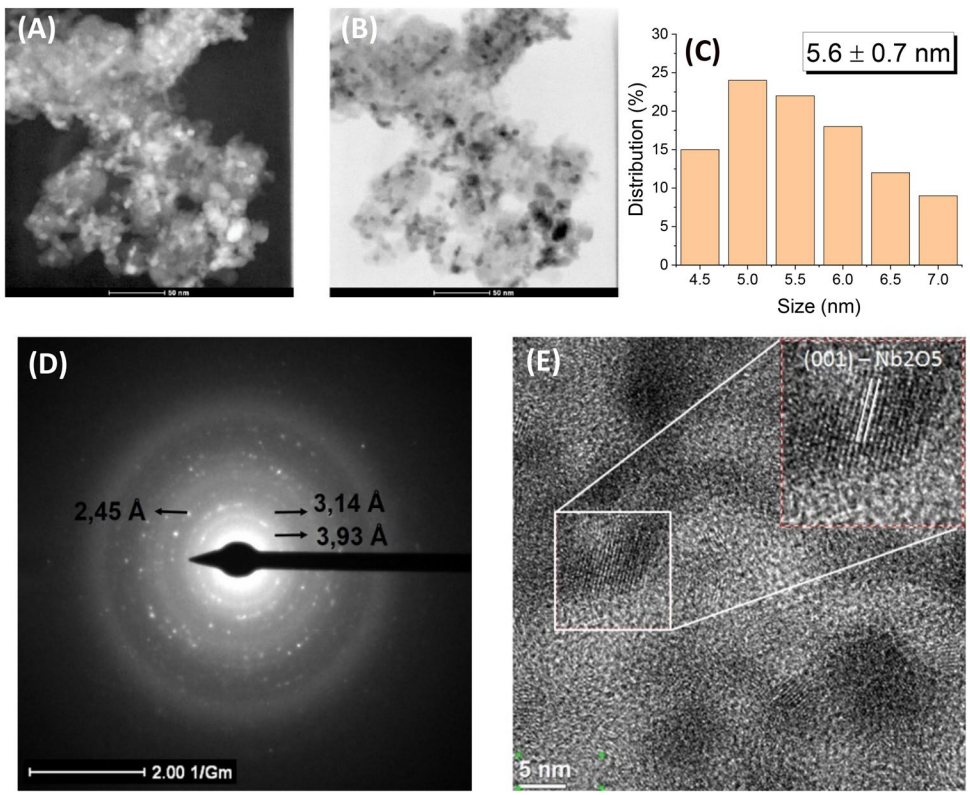

Fig. 2 Transmission electron microscopic image of the Nb_2O_5/C catalyst (5.0 (m/m) Nb/C) in **A** dark field and **B** bright field; **C** histogram of the estimated mean particle size; **D** electron diffraction pattern related to the main crystal planes of the Nb_2O_5 structure; and **E** transmission electron microscopic image with high resolution and Fourier transform refinement

role in the kinetics of oxygen reduction reaction (ORR) in terms of electrocatalytic activity.

The atomic concentrations of the surface area of the particulate material obtained from the XPS high-resolution spectra are presented in Table 1. According to the XPS data, the electrocatalyst had 13.3% more oxygen than the Printex L6 carbon. A small fraction of the oxygen content was linked to niobium; in fact, the concentration of niobium was found to be lower than expected.

The local bonding structure of the electrocatalyst was investigated through the deconvolution of the Nb 3d, C 1s, and O 1s core level spectrum. Figure 3B and D show the Nb 3d spectrum of the electrocatalyst composed of 5.0% Nb and Printex L6 carbon. The spectrum was fitted with good precision by only one spin-orbit doublet at a fixed separation of 2.7 eV with the area ratio of 3:2. The characteristic binding energy of 207.8 eV (Nb $3d_{5/2}$) corresponds to the Nb_2O_5 oxidation state [31, 36]; this is in line with the XRD diffraction patterns.

Figure 3 shows the XPS C 1s and O 1s spectra of 5.0% Nb_2O_5/C electrocatalyst and Printex L6 carbon. Looking at Fig. 3B C, one will observe that the C 1s spectra of 5.0% Nb/C and Printex L6 carbon are composed of four components. The main component of Printex L6 carbon is associated with the aromatic phase (C–C sp^2) at 284.4 eV, and when niobium oxide is added to the Printex L6 carbon support, one notices a reduction in this phase due to the oxidation of the C–C group, which makes the structure more reactive toward ORR [31]. The spectra also show peaks related to the hydrocarbon phase (C–H sp^3) at 285.7 eV and oxidized carbon phases in the form of alcohol/ether at 287.0 eV (C–O) and carboxyl at 289.5 eV (O–C=O).

The main components of the O 1s spectrum (Fig. 3D and E) related to Printex L6 carbon can be linked to the C–O and O–C=O groups at 532.7 and 534.0 eV, respectively; these groups are also identified in the analysis of the C 1s spectrum [22, 31]. A small component observed at high binding energy, 535.8 eV, is associated with molecular water on the surface of the particles. The O 1s spectrum of the 5.0% Nb/C electrocatalyst shows an additional band at low binding energy, which is related to Nb–O bonds at 530.9 eV.

Table 1 Atomic concentration of the surface area of Printex L6 carbon and 5.0% Nb_2O_5/C (w/w) electrocatalyst obtained from XPS high-resolution spectra

Element	Concentration (at.%)	
	Printex L6	Nb/C
Carbon (C 1s)	90.5	77.0
Oxygen (O 1s)	9.5	22.8
Metal (Nb 3d)	–	0.2

3.2 Electrochemical characterization

The cyclic voltammograms obtained for Printex L6 carbon, 5.0% Nb_2O_5/C, and 15% Nb_2O_5/C electrocatalysts are shown in Figure S2. The voltammetric behavior of Printex L6 carbon is characterized by a potential range limited by oxygen evolution reaction (anodic limit) and hydrogen evolution reaction (cathodic limit). One can observe a significant variation in the value of the current at more negative potentials (− 0.4 to − 0.6 V vs. Ag/AgCl) at the beginning of the hydrogen evolution reaction; this variation is attributed to the reduction of H^+ ions present in the solution. The absence of current peaks throughout the potential range studied indicates that the observed currents are of capacitive nature.

The 5.0% Nb/C electrocatalyst displays a blurred peak around 0.2 V vs. Ag/AgCl (I), which is probably associated with Nb (V)/Nb (IV) redox transition—i.e., Nb_2O_5/NbO_2 [31]. The voltammogram obtained for the 15% Nb/C electrocatalyst shows the occurrence of an additional oxide reduction process around − 0.5 V vs. Ag/AgCl (II), which is probably related to redox transition from Nb(IV) to Nb(II)—i.e., NbO_2/NbO [22, 31]. The cathodic current associated with such a process is not visible due to the variation of the current in this potential range at the beginning of the hydrogen evolution reaction.

The voltammogram shows a decrease in the loads associated with the redox transition, i.e., the active area. It can be assumed that electrocatalysts containing lower contents of modifier exhibit smaller crystallite sizes since the intensity of the peaks related to the metal oxide in the XRD decreases when the concentration of the metal is decreased; thus, these electrocatalysts exhibit poor lattice arrangement - i.e., smaller crystallization.

Figure S3 shows the RRDE curves related to the oxygen reduction reaction obtained from the application of carbon with different niobium loadings and Printex L6 carbon. Figure S4 shows the result obtained from the application of carbon with 20% Pt (C/Pt—ETEK). The reactions that take place during the LSV using the RRDE are [30, 36–38]:

$$O_2 + 2H^+ + 2e^- \rightarrow H_2O_2, \quad (1)$$

$$H_2O_2 + 2H^+ + 2e^- \rightarrow 2H_2O, \quad (2)$$

$$O_2 + 4H^+ + 4\,e^- \rightarrow 2H_2O, \quad (3)$$

$$2H^+ + 2e^- \rightarrow H_2 \quad (4)$$

The ORR analysis was performed using carbon modified with Nb_2O_5 and two reference materials—Printex L6 carbon as a reference for the 2-electron ORR mechanism and C/Pt as a reference for the 4-electron ORR

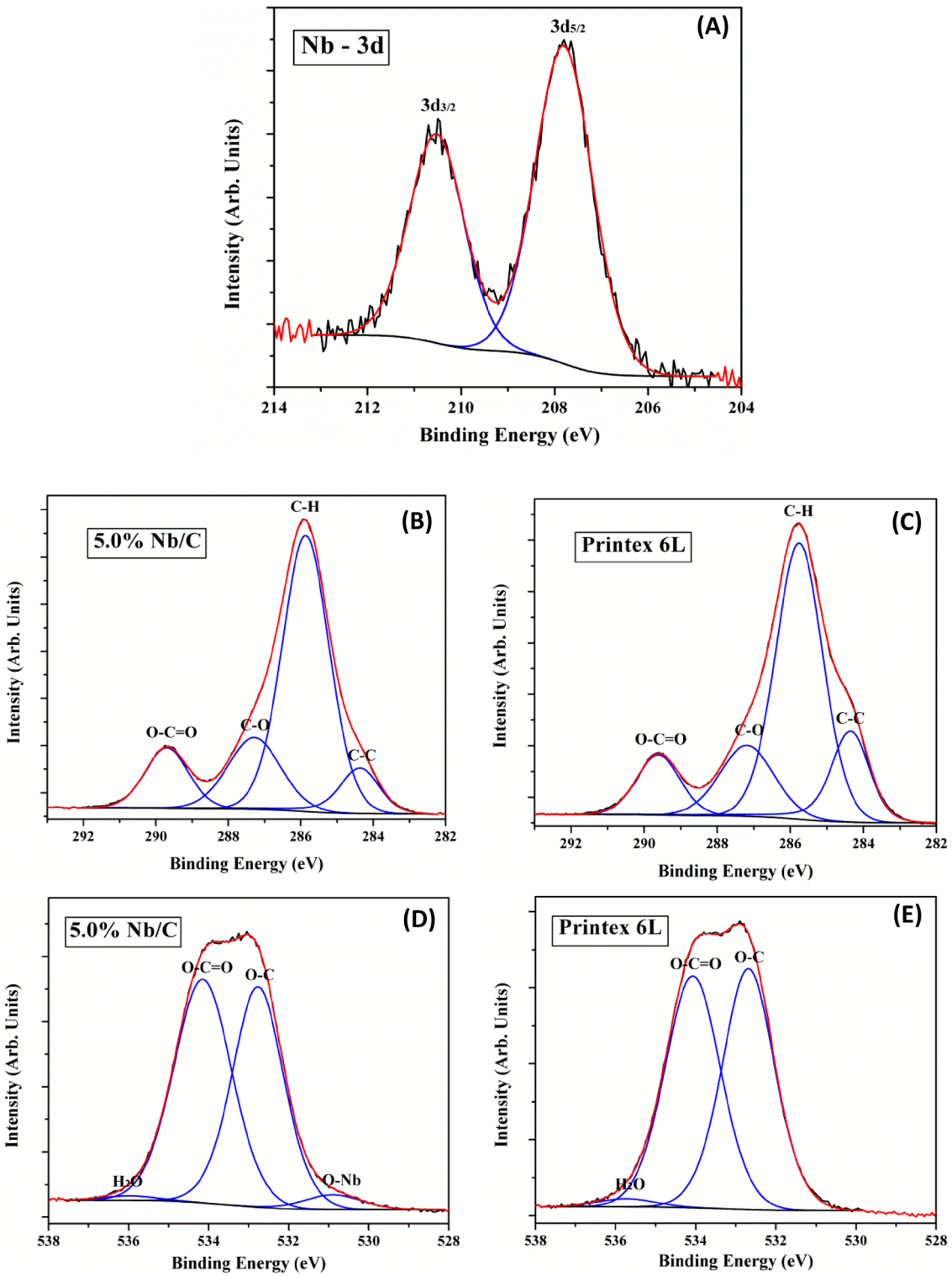

Fig. 3 **A** Deconvoluted XPS Nb 3d spectra of niobium oxide nanoparticles composed of 5.0% Nb_2O_5/C (w/w). Deconvoluted XPS C 1s spectra of **B** 5.0% Nb_2O_5/C (w/w) electrocatalyst and **C** Printex L6 carbon. Deconvoluted XPS O 1s spectra of **D** 5.0% Nb_2O_5/C electrocatalyst and **E** Printex L6 carbon

mechanism. Figure S3 shows the linear sweep voltammograms obtained for the carbon-based materials investigated in the presence and absence of the modifiers. For all the materials investigated, the experiments were initiated at 0.4 V vs. Ag/AgCl and proceeded toward more negative potentials. The ORR (Eq. 1) began at approximately 0.0 V vs. Ag/AgCl (depicted by the increase in the ring current); this shows that the addition of any amount of Nb_2O_5 does not significantly interfere with the onset potential of ORR. Other studies reported in the literature which employed Nb_2O_5 as a carbon modifier under similar experimental conditions also noted that Nb_2O_5 does not modify the onset potential of ORR [22, 31, 36].

As can be noted in Figure S3, while the incorporation of niobium oxide into carbon leads to an increase in the current of the disk, the values of the currents recorded for the materials containing Nb_2O_5 were found to be close to those of Printex L6 carbon. Regarding the ring current response, an increase in current is observed up to 5% Nb_2O_5 mass concentration. After that, one notices a reduction in the H_2O_2 oxidation current; this decrease in current shows that the application of higher concentrations of Nb_2O_5 yields less amount of H_2O_2, which might mean that other parasite reactions (Eqs. 2 and 3) start to occur in greater quantities [30, 36, 37, 39], meaning that the 4 electrons pathway starts to become preferable when the Nb_2O_5 amounts are much higher.

Figure S3 shows the results obtained from the application of 15% Nb_2O_5/C. As can be observed, when applied at the potential ranging from 0.0 to − 0.4 V vs. Ag/AgCl, the 15% Nb_2O_5/C electrocatalyst exhibited patterns of behavior in terms of disk and ring currents, which were quite similar to the unmodified carbon material. However, when applied at the potential ranging from − 0.4 to − 0.8 V vs. Ag/AgCl, the disk current of the 15% Nb_2O_5/C electrocatalyst was found to be greater than that of the unmodified carbon, but the ring current of the former was found to be smaller than that of the latter. Interestingly, this behavior was not observed for the other materials investigated; essentially, this may be an indication that, at more negative potentials, the application of higher amounts of Nb_2O_5 (greater than 10% w/w) may push the ORR closer to a 4-electron mechanism (i.e., higher current in the disk (higher ORR) and lower current in the ring (lower H_2O_2 generation)).

Figure S3 shows the current profiles of the materials investigated. As can be observed, 5% Nb_2O_5/C exhibited the highest H_2O_2 detection current at − 0.5 V vs. Ag/AgCl. It must be noted, however, that for a complete analysis, one needs to also take into account the current applied in ORR at the same potential. According to Valim et al., due to the complexity of ORR analysis when it comes to H_2O_2 formation using the disk and ring currents, the use of equations to calculate the fraction of H_2O_2 detection current in total disk current and the total number of electrons is a viable alternative for evaluating the quality of the materials for H_2O_2 generation [27].

Several studies reported in the literature have used equations to estimate the current efficiency of H_2O_2 formation ($eff_{H_2O_2}$%) and the total number of electrons exchanged (n_t) for each studied material [27]. Based on the current values presented in Figures S3 and S4, the values obtained for $eff_{H_2O_2}$% and n_t are shown in Table 2.

As can be observed in Table 2, Printex L6 carbon recorded a current efficiency for hydrogen peroxide electrogeneration of 76.3; in other words, the application of this material resulted in 76.3% of hydrogen peroxide generation and 23.7% of other reactions. Furthermore, Printex L6 carbon recorded a transfer of 2.5 electrons per oxygen molecule. Pt/C—which is the reference material for ORR via the four-electron pathway, recorded $eff_{H_2O_2}$% of 0.4% and n_t of 3.9.

The 5.0% Nb_2O_5/C (w/w) electrocatalyst exhibited the highest rate of H_2O_2 electrogeneration (82.5%); this is consistent with the polarization curve in which this electrocatalyst recorded higher ring current and smaller disk current compared to the electrocatalyst composed of 3.0% Nb_2O_5/C. In addition, the 5.0% Nb_2O_5/C electrocatalyst exhibited the lowest number of electrons transferred during oxygen reduction.

The high catalytic activity of the electrocatalysts can be associated with the occurrence of redox transition in the cyclic voltammetry. According to previous studies reported in the literature [27], the catalytic activity of the transition oxides is related to the occurrence of redox reaction between the species, such as Nb (V)/Nb (IV), and this reduces the

Table 2 Current efficiency of H_2O_2 formation ($eff_{H_2O_2}$%) and the total number of electrons exchanged (n_t) during ORR using different nominal loadings (w/w) of niobium oxide in carbon and Pt/C

	Printex L6 (− 0.70 V)	0.5% Nb_2O_5/C (− 0.57 V)	1.0% Nb_2O_5/C (− 0.57 V)	3.0% Nb_2O_5/C (− 0.45 V)	5.0% Nb_2O_5/C (− 0.54 V)	8.0% Nb_2O_5/C (− 0.47 V)	10.0% Nb_2O_5/C (− 0.44 V)	15.0% Nb_2O_5/C (− 0.49 V)	Pt/C (− 0.05 V)
$eff_{H_2O_2}$%	76.3	74.6	75.5	76.4	82.5	70.2	68.0	64.1	0.4
n_t	2.5	2.5	2.5	2.5	2.3	2.6	2.6	2.7	3.9

species with the largest number of oxidation, with the subsequent transfer of an electron to oxygen. Apart from the presence of redox species, ORR can be related to the weak strength of adsorption of oxygen to the metal due to the low center of the energy band or low density of occupied electron states in the electrocatalysts near the Fermi level [22, 31]. This adsorption hinders the breaking of the O–O bond, resulting in the formation of hydrogen peroxide as the final product of the reaction, as described in the Pauling model. It is also worth noting that the acidic character of the carbon surface modified with 5% niobium oxide can lead to an increase in the production of hydrogen peroxide due to conductivity and hydrophilic effects.

3.3 Electrochemical generation of H_2O_2 in GDE

In previous results presented above, based on the values of the disk/ring current (Fig. 5), the modification of carbon with Nb_2O_5 was found to lead to significant improvements in H_2O_2 generation, and the 5% C/Nb_2O_5 electrocatalyst was found to generate the highest amount of H_2O_2 among the materials evaluated. It should be noted, however, that the RRDE technique compares ORR currents (disk) and electrochemical detection of H_2O_2 (ring); as such, it points to the tendency for H_2O_2 generation for each material investigated.

Although the RRDE technique can provide us with reliable information regarding the tendency for the electrochemical generation of H_2O_2, one cannot use it to quantify the amount of H_2O_2 generated. Thus, the GDEs were constructed in the presence and absence of 5% Nb_2O_5 for the generation and quantification of H_2O_2 as a function of the applied current (see Fig. 4). For the analysis of H_2O_2 generation, experiments were performed at different current densities where H_2O_2 concentration was evaluated as a function of

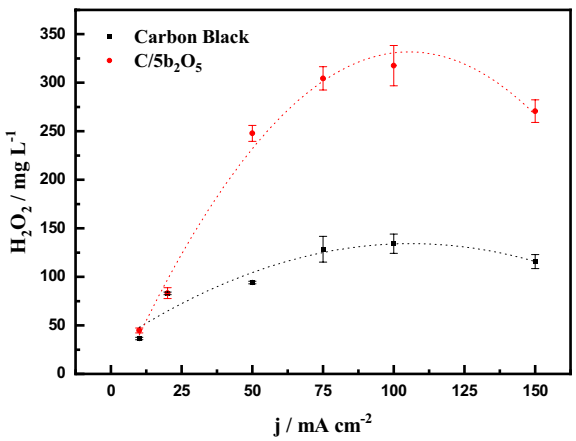

Fig. 4 Variation in the final concentration of H_2O_2 as a function of applied current density based on the application of the unmodified GDE and 5% Nb_2O_5-modified GDE. O_2 pressure applied in the GDE: 0.2 bar. Electrolyte employed: 400 mL of 0.1 mol L^{-1} K_2SO_4 at pH 2

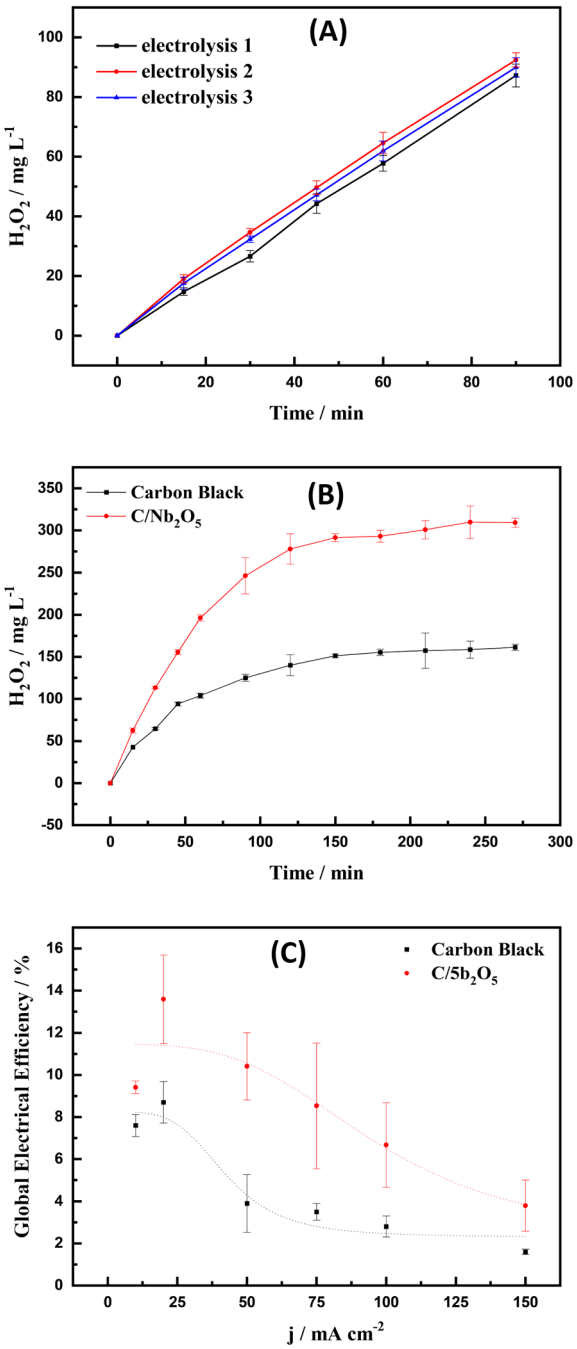

Fig. 5 Stability of the carbon modifier. **A** A sequence of three electrolyzes conducted at the current density of 20 mA cm^{-2} using the same modified GDE. **B** Long-term electrolysis (270 min) conducted using unmodified GDE and 5% Nb_2O_5-modified GDE, both applied at the current density of 100 mA cm^{-2}. **C** Variation in global efficiency of H_2O_2 generation as a function of applied current density based on the application of unmodified GDE and 5% Nb_2O_5-modified GDE after 90 min of electrolysis. O_2 pressure applied in GDE: 0.2 bar. Electrolyte employed: 400 mL of 0.1 mol L^{-1} K_2SO_4 at pH 2

time. The results obtained from the experiments showed that H_2O_2 concentration increased linearly as a function of time. The results obtained from the analysis involving H_2O_2 concentration as a function of time can be found in Figures S5 and S6 in the Supplementary Material.

Figure 4 shows variation in the final concentration of H_2O_2 generated in the experiments conducted using 5% Nb_2O_5-modified GDE and unmodified GDE. See Figures S5 and S6 for the final H_2O_2 concentrations obtained

The two main points observed in this experimental analysis were as follows: (i) first, the incorporation of Nb_2O_5 in carbon (100 mA cm^{-2}) led to a significant increase in H_2O_2 generation, with the production of 317.6 mg L^{-1} of H_2O_2; this amount represents an increase of 136.8% in the amount of H_2O_2 generated in comparison with the H_2O_2 generated under the application of the unmodified GDE (134.1 mg L^{-1}) using the same experimental conditions. As pointed out by Valim et al. [27], the variation in H_2O_2 concentration between different electrodes of the same composition with the application of the same experimental conditions is $4.5 \pm 0.4\%$. The increase in H_2O_2 generation fueled by the incorporation of Nb_2O_5 is higher than the intrinsic variation of the GDE [20]; (ii) secondly, the application of both the Nb_2O_5-modified GDE and the unmodified GDE at the current density of 150 mA cm^{-2} led to a decrease in the final concentration of H_2O_2; this behavior may be associated with the amount of energy supplied to the system, which stimulated a greater occurrence of parallel reactions (Eqs. 2–4) and led to the detection of a lower concentration of H_2O_2 at the end of the experiments.

The results presented in Fig. 4 show a dependence between H_2O_2 generation and applied current density for the modified and unmodified electrodes. To gain a better understanding of the analytical efficiency of the electrodes, it is crucial to evaluate the stability of the carbon modification process. Given that, relevant analytical tests were performed. The first test evaluated the reproducibility of H_2O_2 generation in three sequential electrolyzes using the same electrode and new electrolyte in each electrolysis (see Fig. 5A). The second test evaluated H_2O_2 generation in a long-term experiment (270 min) based on the application of new electrodes; the results obtained are shown in Fig. 5B.

One of the key characteristics of the process of H_2O_2 generation in porous electrodes is reproducibility [20]. Figure 5A shows the concentration of H_2O_2 obtained from the three electrolyzes conducted using the same GDE and new electrolyte for each electrolysis. As can be observed, the H_2O_2 concentration values obtained in the three experiments were quite similar, with a variation of $2.3 \pm 0.4\%$ under the treatment periods investigated. Interestingly, the variation in H_2O_2 concentration observed in this study is very close to the variation reported by Reis et al. [20]; this points to the reproducibility of the C/Nb_2O_5-modified GDE.

Figure 5B presents the results obtained from the long-term H_2O_2 generation experiments conducted using the unmodified GDE and the 5% Nb_2O_5-modified GDE. The objective of these experiments was to evaluate the stability of H_2O_2 generation throughout the experiments with the modification of carbon. The results obtained from the experiments conducted using both electrodes showed that, after 150 min of experiment, the variation in H_2O_2 concentration as a function of time stabilizes, with a very small variation in H_2O_2 concentration observed after this period up to the end of the experiment. The 5% Nb_2O_5-modified GDE and the unmodified GDE recorded final H_2O_2 concentrations of 309 and 161 mg L^{-1}, respectively, at the end of the experiments.

The results obtained from these experiments pointed to the reproducibility and stability of the process involving the modification of carbon and H_2O_2 generation in different experimental conditions; in addition, the results also showed that H_2O_2 generation occurred in both unmodified carbon and Nb-modified carbon. The reproducibility (Fig. 5A) and stability (Fig. 5B) observed in the H_2O_2 generation process show that the physical structure and electrochemical property of the electrocatalyst play an effectively constant role in O_2 reduction for H_2O_2 generation; in essence, this points to the success of the process involving the modification of carbon with thermal oxide. For the analysis of the electrochemical activity of Nb in carbon, the global electrical efficiency for H_2O_2 generation was estimated; the results obtained from this analysis are shown in Fig. 5C.

Figure 5C presents the global electrical efficiency values for H_2O_2 generation obtained from the application of the unmodified GDE and Nb_2O_5-modified GDE. For the calculation of the electrical efficiency, both the theoretical and practical numbers of moles of H_2O_2 were considered. The number of theoretical moles was calculated based on the electric charge (applied current and treatment time) and considering that Eq. 1 theoretically occurs with 100% efficiency (thus, all the applied electric charge will be used for H_2O_2 generation). The practical number of moles was calculated based on the mass of H_2O_2 quantified in each sample.

It is worth noting that the electrical efficiency values shown in Fig. 5C take into account only the quantified amount of H_2O_2; this is because, due to the structure of the electrochemical cell (single compartment), a certain amount of H_2O_2 generated may be degraded by the system itself, reduced by 2 electrons forming water and/or oxidized on the anode. Since these parallel reactions were expected to occur, the electrical efficiency was calculated taking into account only the quantified H_2O_2; thus, the global electrical efficiency was calculated for each collected sample. The

results obtained from the calculation of the global electrical efficiency as a function of time are shown in Figures S7 and S8.

As can be observed in Fig. 5C, the increase in applied current density led to a decrease in electrical efficiency; this was possibly due to the excess of energy supplied to the system, which tended to increase the occurrence of secondary reactions parallel to H_2O_2 generation. Another point that deserves mentioning is the difference in efficiency between the electrodes investigated; as expected, the modified GDE presented a higher efficiency compared to the unmodified GDE; this behavior is associated with the activity of Nb_2O_5, which promoted greater H_2O_2 generation in the modified electrode (with maximum efficiency of 13.6%) compared to the unmodified electrode (8.7%), though both electrodes were applied under the same experimental conditions, with a current density of 20 mA cm^{-2}.

Considering the results obtained from the experiments conducted in this study, it is clear that the modification of carbon with Nb_2O_5 significantly enhanced H_2O_2 generation. However, the C/Nb_2O_5-GDE, which generated the highest concentration of H_2O_2 (Fig. 4), also presented the lowest global electrical efficiency (Fig. 5C) due to the excess amount of energy consumed in the application of this electrode and the consequent intensification of parallel reactions.

3.4 LEVO degradation using C/Nb_2O_5-GDE

The analysis involving H_2O_2 generation using the modified and unmodified electrodes showed that the addition of Nb_2O_5 promoted a significant increase in H_2O_2 generation (see Fig. 4). As described by Silva et al. [28], the amount of hydroxyl radical (Eq. 5) is directly associated with the degradation process, and in this sense, the amount of H_2O_2 available in the reaction medium can directly interfere with the process involving the degradation of LEVO and the reduction of the organic load. To evaluate the exact relation between the amount of H_2O_2 available in the solution and the degradation process, two experiments were carried out using either pressurized N_2 or O_2 in the GDE.

$$Fe^{2+} + H_2O_2 \rightarrow Fe^{3+} + \cdot OH + {}^{-}OH \quad (5)$$

The use of pressurized N_2 in the GDE prevents the formation of H_2O_2; as such, the degradation process is linked to anodic (platinum screen) oxidation. The use of pressurized O_2 in the GDE promotes H_2O_2 formation; here, the degradation process is the sum of anodic degradation and hydroxyl radical-induced degradation (hydroxyl radical is derived from H_2O_2 in the presence of Fe^{2+})—this summation occurs due to the single compartment of the electrochemical cell.

3.5 Degradation process using pressurized N_2 in the GDE

The use of pressurized N_2 in the GDE inhibited H_2O_2 formation in the reaction medium, and the degradation process was restricted on the surface of the anode; in this sense, the samples were previously taken, and no H_2O_2 concentrations were detected under the current densities investigated.

With regard to the degradation experiments conducted under all the current densities investigated, the results obtained showed that there was no significant decrease in LEVO concentration. A maximum LEVO removal rate of less than 1% was obtained from the application of a current density of 150 mA cm^{-2}; this extremely low removal rate is associated with the small anode area. Based on the results obtained in these experiments, it is clear that the degradation process in the absence of H_2O_2 is irrelevant to the removal of LEVO, and therefore these results are not presented in this study; thus, a thorough analysis was conducted in order to evaluate the percentages of LEVO and organic load removal in the presence of H_2O_2 (by using pressurized O_2 in the GDE) with and without Fe^{2+} ions.

3.6 Degradation process using pressurized O_2 in the GDE

To perform the degradation experiments in the presence of O_2, which promotes H_2O_2 formation, the same parameters employed for the experiments involvingH_2O_2 generation were used (Fig. 4). First, the removal of LEVO was evaluated using electrolytes in the presence and absence of Fe^{2+} ions at different current densities; the values obtained from this analysis are shown in Fig. 6.

Figure 6 A shows the values obtained in terms of LEVO removal based on the application of different current densities. Here, two distinct patterns of behavior can be observed. First, the experiments conducted in the presence of Fe ions resulted in a significant increase in LEVO removal under all the current densities investigated in comparison to the experiments performed in the absence of Fe ions; the experiments conducted in the presence of Fe ions yielded LEVO removal rates between 83 and 91% at current densities of 10 and 150 mA cm^{-2}, respectively. By contrast, as can be observed in Fig. 6, the experiments performed in the absence of Fe ions resulted in relatively lower removal rates of LEVO, where values between 30 and 71% were obtained based on the application of current densities ranging from 10 to 150 mA^{-2}.

A further interesting point that merits mentioning in Fig. 6A has to do with the behavior of the removal rates obtained from the experiments conducted in the presence and absence of Fe^{2+}. For the experiments carried out in the presence of Fe^{2+}, the removal rates obtained at all the current

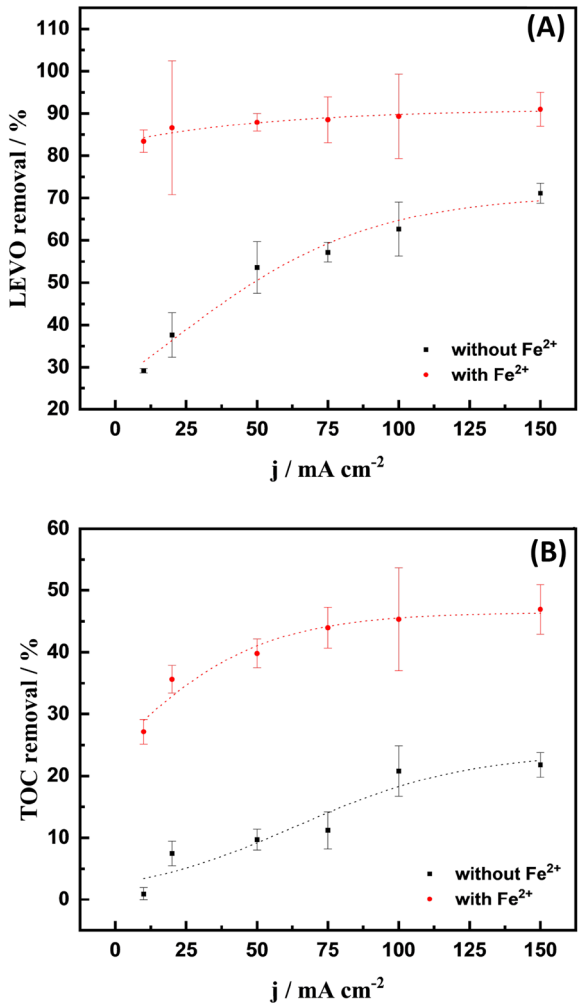

Fig. 6 **A** Variation in LEVO removal; and **B** Variation in TOC removal. Both LEVO and TOC removal percentages were evaluated as a function of applied current density based on the application of unmodified GDE and 5% Nb_2O_5-modified GDE using electrolytes in the presence and absence of ions Fe^{2+} and 10 mg L^{-1} of LEVO. O_2 pressure in GDE: 0.2 bar. The results shown here were based on experiments conducted for 90 min

densities applied were found to be close to one another (minimum of 83% and maximum of 91%); this behavior is associated with the availability of hydroxyl radicals since hydroxyl radicals are immediately formed during the process involving H_2O_2 generation in the presence of Fe^{2+}. This may explain why 83% of the LEVO removal rate was obtained in the experiment that involved lower H_2O_2 generation (10 mA cm^{-2}). A different pattern of behavior was observed for the experiments performed in the absence of Fe^{2+}; there was a considerable increase in the removal rate when the applied current density was increased, with a maximum removal rate of 71% obtained from the application of a current density of 150 mA cm^{-2}.

Looking at the values shown in Fig. 6A, one will notice that, in general, high removal rates of LEVO were recorded, especially for the experiments conducted in the presence of Fe^{2+}; however, one needs to point out that these high removal rates are only associated with the monitoring of the LEVO molecule without taking into account the other compounds present in the commercial products. For this reason, a thorough analysis was conducted in order to evaluate the organic load removal in the degradation experiments; the results obtained from this analysis are presented in Fig. 6B.

The commercial compound LEVO (acquired from Sandoz Brasil) was used for performing the experiments involving LEVO degradation; this product contains 500 mg of LEVO per unit, in addition to various incipient compounds, including lactose, sodium starch glycollide, glycerol dibehenate, hyprolose, and macrogol. Due to the presence of these incipient compounds, the organic load of the samples was monitored during the degradation process conducted in the presence and absence of Fe^{2+} ions using the current densities investigated.

The experiments performed in the presence of Fe^{2+} ions led to a significant increase in organic load removal. This behavior, which has already been described in the literature [9, 10, 40–42], was expected, and it is associated with the formation of hydroxyl radicals in the H_2O_2 reaction medium. Figure 6B shows the values obtained for total organic removal (TOC) as a function of the applied current density. As can be observed, an increase in applied current density promoted an increase in TOC removal up to 100 mA cm^{-2}; organic load removal rates of 20% and 45% were obtained for the experiments conducted in the absence and presence of Fe^{2+} ions, respectively.

With regard to the experiments conducted using the applied current density of 150 mA cm^{-2}, the TOC removal rates obtained were 46% and 20% for the experiments carried out in the presence and absence of Fe^{2+} ions, respectively. These results show that a 50% increase in energy applied to the system did not promote greater removal of TOC; this outcome may be associated with the following factors: (i) the amount of organic matter originally present in the samples (initial TOC value of 965 mg L^{-1}); (ii) the amount of H_2O_2 generated in the experiment at 150 mA cm^{-2} (Fig. 6B); and (iii) the duration of the experiment (90 min). In view of that, an experiment was carried out for a period of 270 min in order to gain a better understanding of the process involving the degradation of LEVO and the removal of organic load; the results obtained are shown in Fig. 7.

Figure 7 shows the values obtained in terms of the removal of LEVO and organic load for the experiment conducted at the current density of 100 mA cm^{-2} in the presence of Fe^{2+}. The aforementioned parameters were chosen because the application of these parameters yielded the best results (see Fig. 6A and B) in terms of LEVO and organic load removal; in fact, although the application of a current density of 150 mA cm^{-2} involved the use of a higher amount

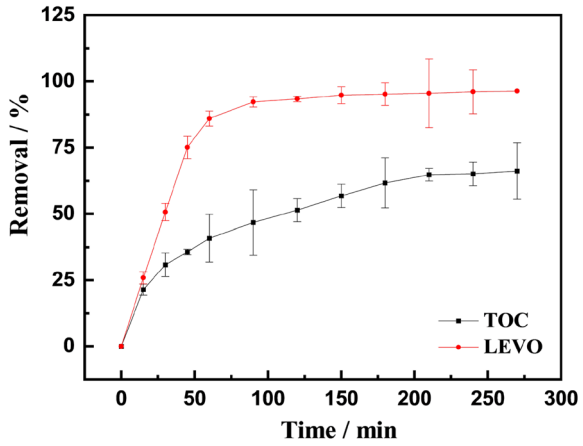

Fig. 7 Long-term electrolysis (270 min) based on the application of 5% Nb_2O_5-modified GDE at a current density of 100 mA cm^{-2}. O_2 pressure in GDE: 0.2 bar. Electrolyte: 400 mL of 0.1 mol L^{-1} K_2SO_4 (at pH 2) in the presence of Fe^{2+} and 10 mg L^{-1} of LEVO

of energy, it yielded the same results as the application of current density of 100 mA cm^{-2}.

The results obtained from this experiment showed that 92% of LEVO removal was obtained after 90 min of treatment (See Fig. 7), with a maximum removal rate of 96% after 270 min of treatment. Regarding TOC removal, 46 and 66% (maximum) of TOC removal rates were obtained after 90 min (see Fig. 7) and 270 min of treatment. These results show that the limitations observed in terms of LEVO and TOC removal (as observed in Figs. 6A and 7) were associated with the duration of the experiment; the increase in degradation time led to a slight increase in LEVO removal (from 91 to 96%) and a considerable increase in TOC removal (from 46 to 66%). Clearly, the results obtained point to a direct relation between a decrease in organic load and the duration of the experiment; this relation can be attributed to the different types of organic structures that constitute the incipient compounds present in the commercial compound.

The results obtained from the experiments involving H_2O_2 generation (Fig. 4) and LEVO degradation (Figs. 6 and 7) showed that the proposed GDE is efficient when applied in H_2O_2 generation, as well as in the degradation of LEVO and the removal of organic load in the samples investigated. Furthermore, while a maximum LEVO removal rate of 92% was obtained after approximately 90 min of degradation, a longer experiment time was required (270 min) to reach a maximum TOC removal of 66%; this outcome was found to be linked to the time of experiment and not to H_2O_2 concentration, since the results obtained from a longer period of the experiment (Fig. 7) showed that H_2O_2 concentration varied very little after 150 min onward while the rate of TOC removal continued to increase up to the end of the experiment period (270 min). Essentially, the results obtained from the experiments conducted in this study point to the following: (i) the amount of H_2O_2 present in the reaction medium was sufficient, and (ii) more time was needed to oxidize the different chemical structures of the incipient compounds present in the commercial product investigated.

4 Conclusion

The present study showed the successful modification of Printex L6 carbon with niobium oxide; this modification allowed us to obtain the C-Nb_2O_5 phase, confirmed by the presence of (001) and (180) crystallographic planes (main), confirmed in the TEM analysis by the interplanar distances 3.93 and 3.14Å, respectively. The results obtained from the analysis of H_2O_2 generation using carbon-based materials modified with different amounts of Nb_2O_5 showed that maximum amounts of H_2O_2 were obtained at the current density of 100 mA cm^{-2}; the application of unmodified GDE and 5% Nb_2O_5-modified GDE led to the generation of 134 and 317 mg L^{-1} of H_2O_2, respectively after 90 min.

Based on the results obtained from the H_2O_2 generation process, experiments were carried out to degrade LEVO in the samples investigated. The application of Nb_2O_5/C-based GDE resulted in LEVO removal of approximately 91% and TOC removal of 46% after 90 min of experiment in the presence of 0.1 mmol L^{-1} $FeSO_4$. In experiments with longer duration, LEVO removal of approximately 96% and TOC removal of 66% were obtained after 270 min of treatment.

The results obtained in this study show that carbon can be successfully modified with niobium oxide, and this niobium oxide/carbon-based material can be used for the generation of H_2O_2 and for the efficient degradation of pharmaceutical compounds.

Supplementary Information The online version contains supplementary material available at https://doi.org/10.1007/s10800-023-01975-z.

Acknowledgements The authors are sincerely grateful to the Brazilian research funding agencies, including the Brazilian National Council for Scientific and Technological Development - CNPq (Grants No. 465571/2014-0, 302874/2017-8, and 427452/2018-0), São Paulo Research Foundation (FAPESP – Grants #2011/14314-1, #2014/50945-4, #2013/02762-5, #2019/00239-0, #2021/12053-8 and #2017/10118-0) and the Coordenação de Aperfeiçoamento de Pessoal de Nível Superior (CAPES – Finance Code 001) for the financial support granted in the course of this research.

Author contributions RBV: Investigation, Methodology, Validation, Formal analysis, Writing. JFC: Investigation, Methodology, Validation, Formal analysis. FLS: Methodology, Formal analysis. JCL: Methodology, Formal analysis, Writing. PH: Methodology, Formal analysis. MCS: Methodology, Formal analysis. RB: Conceptualization, Formal analysis, Resources, Supervision. MRVL: Conceptualization, Resources, Supervision. RSR: Conceptualization, Validation, Resources, Writing, Supervision.

Data availability Data will be made available upon request.

Declarations

Conflict of interest The authors have no competing interests to declare that are relevant to the content of this article.

References

1. Pereira Matias T, Tambasco Maesteghin L, Maria Imperador A (2020) A sustentabilidade ambiental: da utopia à emergência. Rev Bras Educ Ambient 15:160–174. https://doi.org/10.34024/REVBEA.2020.V15.10830
2. Larsen TA, Gujer W (1997) The concept of sustainable Urban water management. Water Sci Technol 35:3–10. https://doi.org/10.1016/S0273-1223(97)00179-0
3. Quadra GR, Oliveira H, de Souza R, dos Costa S, dos Fernandez MA (2016) Do pharmaceuticals reach and affect the aquatic ecosystems in Brazil? A critical review of current studies in a developing country. Environ Sci Pollut Res 242:1200–1218. https://doi.org/10.1007/S11356-016-7789-4
4. de Souza RC, Godoy AA, Kummrow F, dos Santos TL, Brandão CJ, Pinto E (2021) Occurrence of caffeine, fluoxetine, bezafibrate and levothyroxine in surface freshwater of São Paulo State (Brazil) and risk assessment for aquatic life protection. Environ Sci Pollut Res 28:20751–20761. https://doi.org/10.1007/S11356-020-11799-5/FIGURES/2
5. Chen Z, Li M, Wen Q (2017) Comprehensive evaluation of three sets of advanced wastewater treatment trains for treating secondary effluent: organic micro-pollutants and bio-toxicity. Chemosphere 189:426–434. https://doi.org/10.1016/J.CHEMOSPHERE.2017.09.092
6. Wielens Becker R, Ibáñez M, Cuervo Lumbaque E, Wilde ML, Flores da Rosa T, Hernández F, Sirtori C (2020) Investigation of pharmaceuticals and their metabolites in Brazilian hospital wastewater by LC-QTOF MS screening combined with a preliminary exposure and in silico risk assessment. Sci Total Environ 699:134218. https://doi.org/10.1016/J.SCITOTENV.2019.134218
7. Santos AV, Fonseca Couto C, Abner Rocha Lebron YA, Moreira VR, Souza Foureaux AF, Oliveira Reis E, de Andrade LH, de Andrade LH, Santos Amaral MC, Lange LC (2020) Occurrence and risk assessment of pharmaceutically active compounds in water supply systems in Brazil. Sci Total Environ 746:141011. https://doi.org/10.1016/j.scitotenv.2020.141011
8. Pivetta RC, Rodrigues-Silva C, Ribeiro AR, Rath S (2020) Tracking the occurrence of psychotropic pharmaceuticals in brazilian wastewater treatment plants and surface water, with assessment of environmental risks. Sci Total Environ 727:138661. https://doi.org/10.1016/J.SCITOTENV.2020.138661
9. Epold I, Trapido M, Dulova N (2015) Degradation of levofloxacin in aqueous solutions by fenton, ferrous ion-activated persulfate and combined fenton/persulfate systems. Chem Eng J 279:452–462. https://doi.org/10.1016/j.cej.2015.05.054
10. Hamdi El Najjar N, Touffet A, Deborde M, Journel R, Leitner NKV (2013) Levofloxacin oxidation by ozone and hydroxyl radicals: kinetic study, transformation products and toxicity. Chemosphere 93:604–611. https://doi.org/10.1016/j.chemosphere.2013.05.086
11. Mustafa FS, Oladipo AA (2021) Photocatalytic degradation of metronidazole and bacteria disinfection activity of Ag-doped $Ni_{0.5}Zn_{0.5}Fe_2O_4$. J Water Process Eng 42:2214–7144. https://doi.org/10.1016/j.jwpe.2021.102132
12. Azalok KA, Oladipo AA, Gazi M (2021) Hybrid MnFe-LDO–biochar nanopowders for degradation of metronidazole via UV-light-driven photocatalysis: characterization and mechanism studies. Chemosphere 268:128844. https://doi.org/10.1016/j.chemosphere.2020.128844
13. Azalok KA, Oladipo AA, Gazi M (2020) UV-light-induced photocatalytic performance of reusable MnFe-LDO-biochar for tetracycline removal in water. J Photochem Photobiol 405:1010–6030. https://doi.org/10.1016/j.jphotochem.2020.112976
14. Wu S, Hu YH (2021) A comprehensive review on catalysts for electrocatalytic and photoelectrocatalytic degradation of antibiotics. Chem Eng J 409:127739. https://doi.org/10.1016/j.cej.2020.127739
15. Chen G, Yu Y, Liang L, Duan X, Li R, Lu X, Yan B, Li N, Wang S (2021) Remediation of antibiotic wastewater by coupled photocatalytic and persulfate oxidation system: a critical review. J Hazard Mater 408:124461. https://doi.org/10.1016/j.jhazmat.2020.124461
16. Ighalo JO, Igwegbe CA, Aniagor CO, Oba SN (2021) A review of methods for the removal of penicillins from water. J Water Process Eng. https://doi.org/10.1016/j.jwpe.2020.101886
17. Rios Miguel AB, Jetten MSM, Welte CU (2020) The role of mobile genetic elements in organic micropollutant degradation during biological wastewater treatment. Water Res X. https://doi.org/10.1016/j.wroa.2020.100065
18. Hassani A, Malhotra M, Karim AV, Krishnan S, Nidheesh PV (2022) Recent progress on ultrasound-assisted electrochemical processes: a review on mechanism, reactor strategies, and applications for wastewater treatment. Environ Res 205:112463. https://doi.org/10.1016/j.envres.2021.112463
19. Ahmadi A, Zarei M, Hassani A, Ebratkhahan M, Olad A (2021) Facile synthesis of iron(II) doped carbonaceous aerogel as a three-dimensional cathode and its excellent performance in electro-fenton degradation of ceftazidime from water solution. Sep Purif Technol 278:1383–5866. https://doi.org/10.1016/j.seppur.2021.119559
20. Reis RM, Beati AAGF, Rocha RS, Assumpção MHMT, Santos MC, Bertazzoli R, Lanza MRV (2012) Use of gas diffusion electrode for the in situ generation of hydrogen peroxide in an electrochemical flow-by reactor. Ind Eng Chem Res. https://doi.org/10.1021/ie201317u
21. Ragnini CAR, Iglia RAD, Bertazolli R (2001) Considerações sobre a eletrogeração de peróxido de hidrogênio. Quim Nova 24:252–256. https://doi.org/10.1590/S0100-40422001000200017
22. Carneiro JF, Rocha RS, Hammer P, Bertazzoli R, Lanza MRV (2016) Hydrogen peroxide electrogeneration in gas diffusion electrode nanostructured with Ta_2O_5. Appl Catal A Gen 517:161–167. https://doi.org/10.1016/j.apcata.2016.03.013
23. Rocha RS, Reis RM, Beati AAGF, Lanza MRV, Sotomayor MDPT, Bertazzoli R (2012) Desenvolvimento e avaliação de eletrodos de difusão gasosa (EDG) para geração de H_2O_2 in situ e sua aplicação na degradação do corante reativo azul 19, Quim. Nova 35:1961–1966. https://doi.org/10.1590/S0100-40422012001000014
24. Forti JC, Rocha RS, Lanza MRV, Bertazzoli R (2007) Electrochemical synthesis of hydrogen peroxide on oxygen-fed graphite/PTFE electrodes modified by 2-ethylanthraquinone. J Electroanal Chem 601:63–67. https://doi.org/10.1016/j.jelechem.2006.10.023
25. Assumpão MHMT, Moraes A, De Souza RFB, Gaubeur I, Oliveira RTS, Antonin VS, Malpass GRP, Rocha RS, Calegaro ML, Lanza MRV, Santos MC (2012) Low content cerium oxide nanoparticles on carbon for hydrogen peroxide electrosynthesis. Appl Catal A Gen. https://doi.org/10.1016/J.APCATA.2011.09.030
26. Rocha RS, Valim RB, Trevelin LC, Steter JR, Carneiro JF, Forti JC, Bertazzoli R, Lanza MRV (2020) Electrocatalysis of hydrogen peroxide generation using oxygen-fed gas diffusion

electrodes made of carbon black modified with quinone compounds. Electrocatalysis 11:338–346. https://doi.org/10.1007/s12678-020-00591-1
27. Valim RB, Reis RM, Castro PS, Lima AS, Rocha RS, Bertotti M, Lanza MRV (2013) Electrogeneration of hydrogen peroxide in gas diffusion electrodes modified with tert-butyl-anthraquinone on carbon black support. Carbon NY 61:236–244. https://doi.org/10.1016/j.carbon.2013.04.100
28. Silva FL, Reis RM, Barros WRP, Rocha RS, Lanza MRV (2014) Electrogeneration of hydrogen peroxide in gas diffusion electrodes: application of iron (II) phthalocyanine as a modifier of carbon black. J Electroanal Chem 722–723:32. https://doi.org/10.1016/J.JELECHEM.2014.03.007
29. Antonin VS, Parreira LS, Aveiro LR, Silva FL, Valim RB, Hammer P, Lanza MRV, Santos MC (2017) W@Au nanostructures modifying carbon as materials for hydrogen peroxide electrogeneration. Electrochim Acta 231:713–720. https://doi.org/10.1016/j.electacta.2017.01.192
30. Valim RB, Trevelin LC, Sperandio DC, Carneiro JF, Santos MC, Rodrigues LA, Rocha RS, Lanza MRV (2021) Using carbon black modified with Nb_2O_5 and RuO_2 for enhancing selectivity toward H_2O_2 electrogeneration. J Environ Chem Eng 9:106787. https://doi.org/10.1016/j.jece.2021.106787
31. Carneiro JF, Paulo MJ, Siaj M, Tavares AC, Lanza MRV (2015) Nb_2O_5 nanoparticles supported on reduced graphene oxide sheets as electrocatalyst for the H_2O_2 electrogeneration. J Catal 332:51–61. https://doi.org/10.1016/j.jcat.2015.08.027
32. Zhang M, Xing M, Dong B, Sun X, Zhang H, Wang C, Zhu H (2023) Preparation of $BiVO_4/CO_3^{2-}$-$Bi_2O_2CO_3$ heterojunctions for enhanced photocatalytic activity in the degradation of levofloxacin under visible light. J Alloys Compd 965:171471. https://doi.org/10.1016/J.JALLCOM.2023.171471
33. Xu T, Tang X, Qiu M, Lv X, Shi Y, Zhou Y, Xie Y, Naushad M, Lam SS, Ng HS, Sonne C, Ge S (2023) Degradation of levofloxacin from antibiotic wastewater by pulse electrochemical oxidation with BDD electrode. J Environ Manage 344:118718. https://doi.org/10.1016/j.jenvman.2023.118718
34. Al Busaidi A, Al Marzouqi F, Kuvarega AT, Sillanpaa M, Selvaraj R (2023) Bimetallic $Cd_xZn_{(1-x)}o$ photocatalytic material for the degradation of levofloxacin under solar light irradiation. Inorg Chem Commun 151:110573. https://doi.org/10.1016/J.INOCHE.2023.110573
35. Jandaghian F, Ebrahimian Pirbazari A, Tavakoli O, Asasian-Kolur N, Sharifian S (2023) Comparison of the performance of Ag-deposited ZnO and TiO_2 nanoparticles in levofloxacin degradation under UV/visible radiation. J Hazard Mater Adv 9:100240. https://doi.org/10.1016/J.HAZADV.2023.100240
36. Trevelin LC, Valim RB, Carneiro JF, De Siervo A, Rocha RS, Lanza MRV (2020) Using black carbon modified with NbMo and NbPd oxide nanoparticles for the improvement of H_2O_2 electrosynthesis. J Electroanal Chem 877:114746. https://doi.org/10.1016/j.jelechem.2020.114746
37. Valim RB, Lourenço JC, Trevelin LC, Siqueira AF, Rodrigues LA, Rocha RS, Lanza MRV (2023) Using GDE modified with mixed Ru-Nb oxides for ciprofloxacin degradation via the electro-fenton process and its prediction model. J Water Process Eng 55:2214–7144. https://doi.org/10.1016/j.jwpe.2023.104113
38. Yeager E (1984) Electrocatalysts for O_2 reduction. Electrochim Acta 29:1527–1537. https://doi.org/10.1016/0013-4686(84)85006-9
39. Trevelin LC, Valim RB, Lourenço JC, De Siervo A, Rocha RS, Lanza MRV (2023) Using ZrNb and ZrMo oxide nanoparticles as catalytic activity boosters supported on printex L6 carbon for H2O2 production. Adv Powder Technol 34:104108. https://doi.org/10.1016/j.apt.2023.104108
40. Liu X, Liu Y, Lu S, Wang Z, Wang Y, Zhang G, Guo X, Guo W, Zhang T, Xi B (2020) Degradation difference of ofloxacin and levofloxacin by UV/H_2O_2 and UV/PS (persulfate): efficiency, factors and mechanism. Chem Eng J 385:123987. https://doi.org/10.1016/j.cej.2019.123987
41. Rocha RS, Valim RB, Trevelin LC, Silva FL, Steter JR, Zaiat M, Lanza MRV (2017) New operational mode of an electrochemical reactor and its application to the degradation of levofloxacin. J Environ Chem Eng 5:4441–4446. https://doi.org/10.1016/j.jece.2017.08.041
42. Ma Q, Zhang H, Zhang X, Li B, Guo R, Cheng Q, Cheng X (2019) Synthesis of magnetic CuO/$MnFe_2O_4$ nanocompisite and its high activity for degradation of levofloxacin by activation of persulfate. Chem Eng J 360:848–860. https://doi.org/10.1016/J.CEJ.2018.12.036

Authors and Affiliations

Ricardo Bertholo Valim[1,2] · Jussara Fernandes Carneiro[1] · Julio César Lourenço[1] · Peter Hammer[3] · Mauro Coelho dos Santos[4] · Liana Alvares Rodrigues[2] · Rodnei Bertazzoli[5] · Marcos Roberto de Vasconcelos Lanza[1] · Robson da Silva Rocha[2]

✉ Marcos Roberto de Vasconcelos Lanza
marcoslanza@usp.br

✉ Robson da Silva Rocha
robson.rocha@usp.br

[1] São Carlos Institute of Chemistry – University of São Paulo, São Carlos, SP 13560-970, Brazil

[2] Lorena School of Engineering – University of São Paulo, Lorena, SP 12602-810, Brazil

[3] Institute of Chemistry, UNESP –São Paulo State University, Araraquara, SP 14801-970, Brazil

[4] Laboratory of Electrochemistry and Nanostructured Materials – Federal University of ABC, Santo André, SP 09210-170, Brazil

[5] Laboratory of Electrochemical Engineering – State University of Campinas, Campinas, SP 13083-860, Brazil